A Frequency-Reconfigurable Radiator-Shared MIMO Antenna for Metal-Bezel Smartphones

Xiujuan Lu, *Student Member, IEEE*, Huan Meng, *Member, IEEE*, and Jiangwei Sui, *Member, IEEE*

.

***Abstract*—This letter presents a frequency-reconfigurable MIMO antenna for metal-bezel mobile phones. The design employs an unbroken metal bezel as a shared radiator to make the differential mode (DM) and common mode (CM) fields present a similar slot mode, facilitating a natural self-decoupling by readily counteracting the two mode impedances. Moreover, benefiting from a similar mode, the DM and CM can be simultaneously tuned to almost the same frequency by adjusting the equivalent length of the shared radiator through varying the loading varactors, achieving inherent frequency-reconfigurable self-decoupling, where the S_{21} and S_{11} can be easily tuned at the same time. An experimental verification demonstrates that within the 5G N79 band from 4.4 to 5 GHz, the proposed antenna can achieve a frequency-reconfigurable decoupling with S_{11} better than -10 dB and S_{21} lower than -20 dB, as well as an average total efficiency of 64.6%.**

***Index Terms*—Antenna decoupling, frequency-reconfigurable, metal bezel, MIMO, radiator-shared, smartphones.**

I. Introduction

SINCE THE iPhone 4 was announced about fifteen years ago to be the first commercial metal-bezel smartphone [1], metal-bezel antennas have attracted considerable attention from both industry and academia [2] – [16]. Among these designs, the frequency reconfigurability is widely constructed by introducing some tuners, such as varactors [11] – [13] and switches [14] – [16], to improve the utilization efficiency of the space and frequency [2].

On the other hand, multiple-input and multiple-output (MIMO) antennas have been extensively adopted in mobile phones, where significant mutual coupling between the antennas is unavoidably generated [17]. To address this issue, various decoupling techniques have been explored. One straightforward solution is to utilize the spatial diversity by enlarging the antenna separation [18]. Besides, incorporating additional decoupling elements or structures also proves effective, such as neutralization structures [19], parasitic units [20], [21], decoupling network [22], [23], feeding networks [24], and lumped decoupling elements [25] – [27].

To further reduce the antenna footprint, the inherent antenna characteristics are exploited to achieve natural self-decoupling without additional decoupling structures. This includes strategically manipulating antenna geometry and structure [28] – [32], exploiting mode orthogonality [33], utilizing pattern and polarization diversity [34], [35], and employing mode cancellation techniques [36]. Additionally, some recent studies investigate the orthogonality between differential-mode and common-mode antennas [37] – [40]. Despite the proven excellent decoupling performance, few of these self-decoupling designs support the reconfigurability of working frequency, since for frequency-reconfigurable decoupling of MIMO antenna, not only the S_{11} but also the S_{21} need to be adjusted simultaneously when varying the tuners.

In this letter, a frequency-reconfigurable radiator-shared self-decoupled antenna is proposed. A 1-λ metal bezel is adopted as the shared radiating body for the antenna pair, with the differential mode (DM) and common mode (CM) sharing a dominant 1/2-λ slot mode and thus similar mode impedances. Therefore, the S_{11} and S_{21} of the proposed antenna can be tuned simultaneously to a certain desired frequency with proper loading of tuners, achieving eventual frequency-reconfigurable self-decoupling.

The core innovations and contributions of this work lie in:

1) Benefiting from the intentionally-designed antenna configuration, the DM and CM share a similar dominant slot mode, so a natural frequency-reconfigurable mode impedance cancellation is achieved, guaranteeing that S_{11} and S_{21} can be simultaneously adjusted by tuning the varactor diode.

2) The slit-free configuration of the proposed antenna not only features a higher mechanical strength as well as better aesthetic appearance, but also provides a complementary solution apart from the traditional antenna with a slit.

II. Antenna Configuration and Working Principles

First, two microstrip lines are directly connected to a slit-free metal bezel to construct a two-port antenna system with a slot cut on the ground, as shown in Fig. 1(a). Based on the DM/CM analysis [36], the scattering parameters of the two-port network can be expressed as follows:

$$S_{11} = \frac{S_{c11} + S_{d11}}{2}, \quad S_{21} = \frac{S_{c11} - S_{d11}}{2} \tag{1}$$

Manuscript received xxxx xx, 2026; accepted xxxx. This work was supported in part by the National Natural Science Foundation of China under Grant 62201625, in part by Guangdong Basic and Applied Basic Research Foundation under Grant 2025A1515010696, and in part by the Science, Technology and Innovation Commission of Shenzhen Municipality under Grant KJZD20240903101314019. (*Corresponding author: Jiangwei Sui.*)

Xiujuan Lu and Jiangwei Sui are with the School of Electronics and Communication Engineering, Shenzhen Campus of Sun Yat-sen University, Shenzhen 518000, China (e-mail: luxj26@mail2.sysu.edu.cn; suijw@mail.sysu.edu.cn).

Huan Meng is with the College of Big Data and Internet, Shenzhen Technology University, Shenzhen 518000, China (email: menghuan@sztu.edu.cn).

This article has been accepted for publication in IEEE Antennas and Wireless Propagation Letters. This is the author's version which has not been fully edited and content may change prior to final publication. Citation information: DOI 10.1109/LAWP.2026.3688769

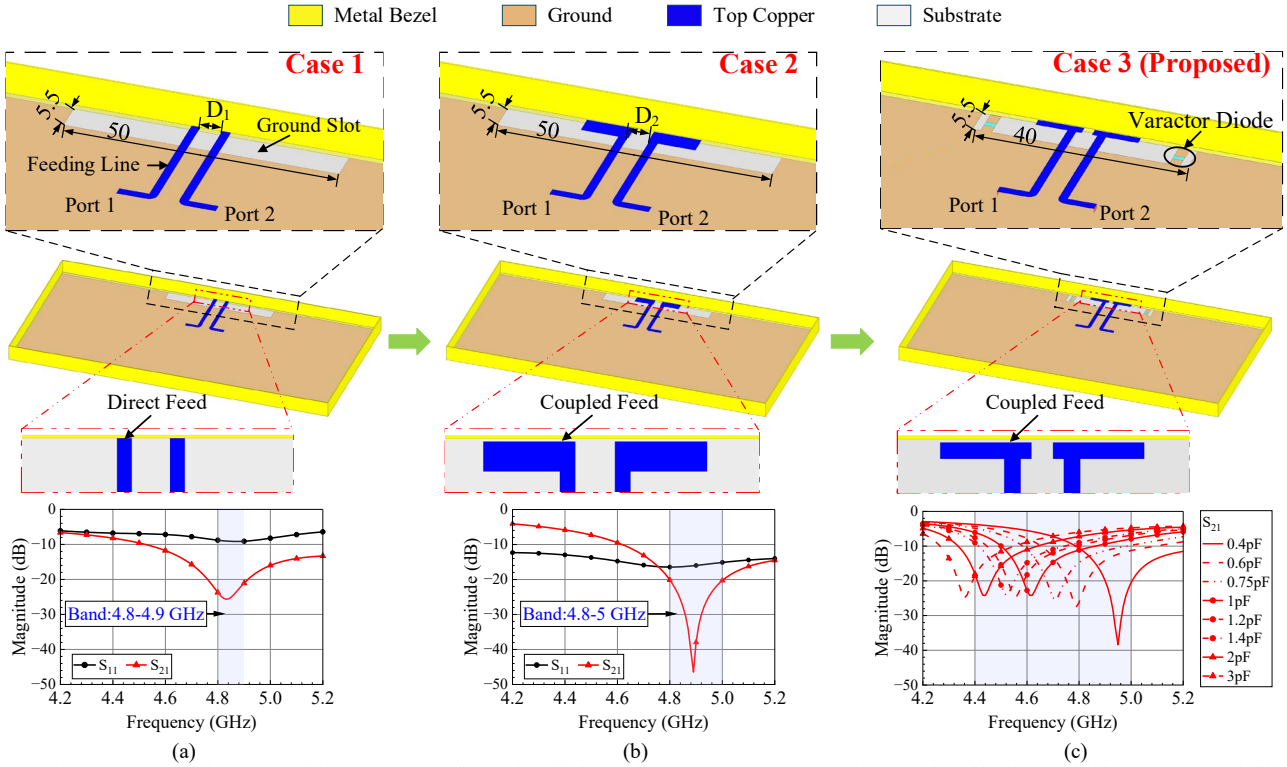

Fig. 1. Evolution process of the proposed frequency-reconfigurable self-decoupled antenna. (a) Case 1: The metal bezel is directly fed by two microstrip lines. (b) Case 2: The metal bezel is coupled-fed by two microstrip branches. (c) Case 3 (Proposed): Two varactor diodes are loaded. (Unit: mm)

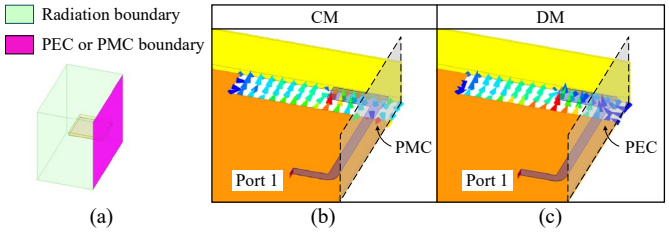

Fig. 2. Electric fields distribution at 4.9 GHz for PMC and PEC boundaries. (a) Boundary description. (b) PMC. (c) PEC.

where S_{c11} and S_{d11} denote the reflection coefficient of the CM and the DM one-port network, respectively, as depicted in Fig. 2. Based on (1), it is easy to derive that the only solution for MIMO antenna decoupling is that both S_{c11} and S_{d11} approach zero, meaning both are near the center of the Smith Chart.

In the simulation for CM analysis, the symmetry plane is set as a perfect magnetic conductor (PMC) boundary, while for DM analysis, it is a perfect electric conductor (PEC) boundary. It is observed that for both the PMC and PEC boundaries, the electric field distribution of the ground slot presents a similar typical 1/2 λ slot mode at the center frequency of 4.9 GHz. Although the field distributions of these two modes near the symmetrical plane exhibit a slight difference, the electric field magnitude is too small to affect the dominant 1/2 λ mode, so the total electric field distributions of the two modes present a high degree of similarity.

Simulated S-parameters in Fig. 1(a) demonstrate that this design achieves 20 dB isolation within the band from 4.8 to 4.9 GHz. However, the decoupling bandwidth is not so wide, and the S_{11} is also worse than -10 dB. To improve decoupling bandwidth and matching condition, a coupled feeding design is proposed, as depicted in Fig. 1(b). It is seen that the 20-dB isolation bandwidth is improved from 100 to 200 MHz of 4.8 – 5 GHz, with S_{11} improved to be better than -15 dB.

The effect of ground slot length is then studied. As the length increases, the frequency of S_{c11} and S_{d11} will decrease so that those of S_{11} and S_{21}, which can be deduced from (1). The results in Fig. 3 exactly prove this deduction. Therefore, by loading two varactors at a proper position to tune the equivalent length of the ground slot, a frequency-reconfigurable self-decoupling can be readily constructed, as depicted in Fig. 1(c). The input admittance Y_{in} of an open-circuited transmission line is

$$Y_{\text{in}} = \text{j}Y_0 \tan(\beta l), \tag{2}$$

where β is the phase constant, l is the physical length, and Y_0 is the characteristic admittance. Connecting a parallel grounding capacitor C gives the total admittance as follows

$$Y_{\text{total}} = \text{j}Y_0 \tan\left(\beta l'\right) + \text{j}2\pi fC. \tag{3}$$

Equating (2) and (3) shows that the equivalent length can be tuned via adjusting the value of the loading capacitor.

Fig. 4 shows the simulated S_{c11} and S_{d11} on the Smith Chart as the capacitance increases from 0.4 to 2 pF. It is observed that the matching frequencies of S_{c11} and S_{d11} both decrease and almost coincide with each other with the capacitance. According to (1), this simultaneously yields $S_{11}\approx 0$ and $S_{21}\approx 0$, achieving ideal matching and perfect isolation at that frequency, explaining why a single varactor can simultaneously tune both the matching and decoupling frequencies in Fig. 1(c).

III. Antenna Implementation and Discussions

In this part, the proposed frequency-reconfigurable antenna

This article has been accepted for publication in IEEE Antennas and Wireless Propagation Letters. This is the author's version which has not been fully edited and content may change prior to final publication. Citation information: DOI 10.1109/LAWP.2026.3688769

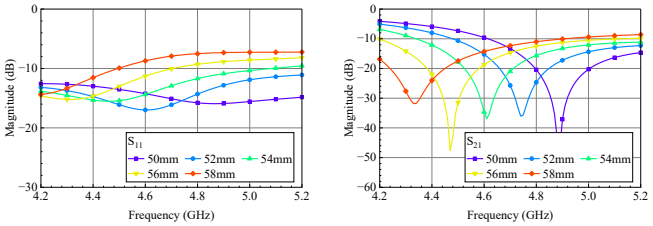

Fig. 3. The effect of the ground slot on the S-parameters. (a) S_{11}. (b) S_{21}.

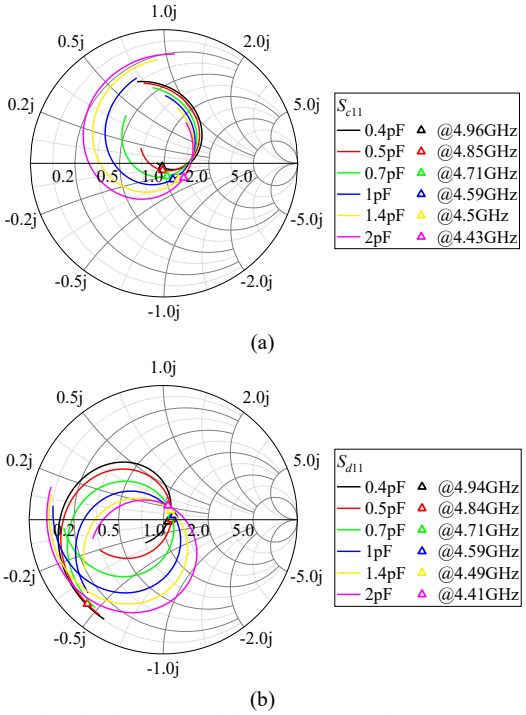

Fig. 4. Simulated reflection coefficient versus capacitance. (a) S_{c11}. (b) S_{d11}.

is implemented, as shown in Fig. 5. In the simulation, the substrate has a relative permittivity of 4.2 and a loss tangent of 0.02. Fig. 6 shows a prototype of the fabricated antenna.

The simulated and measured S-parameters are compared in Fig. 7. In measurement, there are two cases of the loading capacitors: 1) using lumped capacitors of different values one by one; and 2) using two varactor diodes to tune the capacitance by adjusting the loading voltages.

For the measured results in Fig. 7(b), the varying rule of the S-parameters with the capacitor maintains the same as the simulated results in Fig. 7(a), and within the N79 band from 4.4 to 5 GHz, the mutual coupling S_{21} can be controlled to be below -20 dB with S_{11} better than -10 dB.

Furthermore, two varactor diodes of series SMV2020-079LF from Skyworks, which feature a capacitance range of 0.35 to 3.2 pF over a reverse bias voltage range of 0 to 20 V, are adopted to achieve the electronic tuning. A figure of the test system is inserted in Fig. 7(c). Measured results in Fig. 7(c) indicate that when the bias voltage is adjusted, the antennas achieve port isolation better than 20 dB within the 4.4 – 5 GHz band, with the S_{11} lower than -10 dB.

The measured total efficiencies shown in Fig. 8 justify an average total efficiency of 64.6% within the desired band. Besides, simulations were conducted with series resistances of

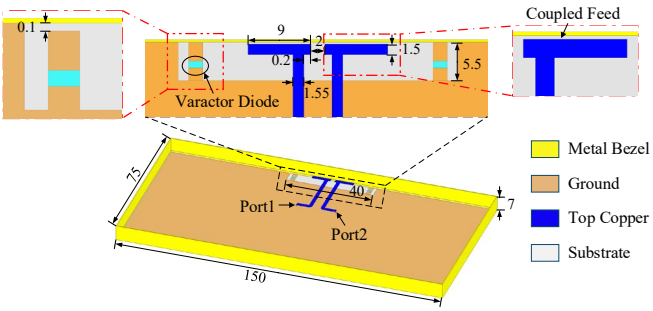

Fig. 5. Detailed configuration of the proposed antenna. (Unit: mm)

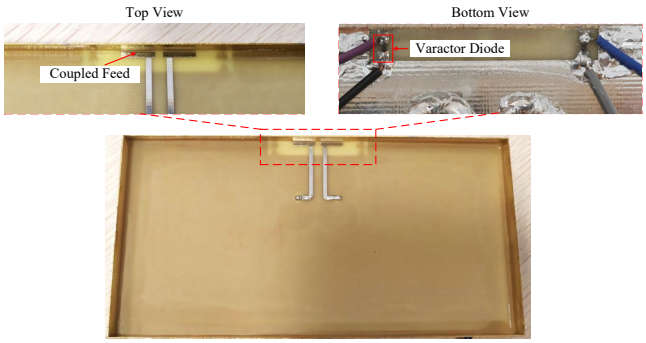

Fig. 6. A photograph of the fabricated prototype of the proposed antenna.

0 Ω (ideal capacitor), 0.7 Ω (typical lumped capacitor), and 2.5 Ω (typical varactor diode), achieving radiation efficiencies of 78.4%, 73.6%, and 67.1%, respectively. The average efficiency fluctuation between adjacent tuning states is within 5% for the 2.5 Ω case, demonstrating stable performance. Fig. 9 presents the measured radiation patterns at 4.9 GHz, demonstrating a good spatial diversity for MIMO applications.

The envelope correlation coefficient (ECC) is below 0.05 across the entire band, and the channel capacity achieved by the proposed antenna is very close to the ideal 2×2 MIMO capacity, indicating a promising MIMO performance, demonstrating excellent MIMO performance. User interaction was investigated using a typical hand model of talking/holding posture. While total efficiency degrades due to hand absorption, it remains above 46% in the worst-case centered position, and improves to over 64% when the antenna is shifted 40 mm away from the center. Besides, the proposed antenna can be in other configurations and bands, for example, the N78 band, N41 band, and a perpendicular configured one in the N79 band [41].

It is seen from Table I that although the frequency reconfigurability is achieved in [14], [16], and [18], the design in [14] and [16] focuses on the single antenna scenario, and the design in [18] only addresses the tuning of S_{11} with isolation obtained by a large antenna separation. For the other works of metal-bezel antenna, although good performance is achieved for MIMO application [37], [39], [40], they all lack the frequency-reconfigurable capability to support service feasibility. In contrast, this work presents a frequency-reconfigurable MIMO antenna that simultaneously tunes S_{11} and S_{21}, providing a promising frequency-reconfigurable MIMO antenna solution in metal-bezel smartphones. Although the footprint of the proposed antenna is a little larger, the slit-free feature of the

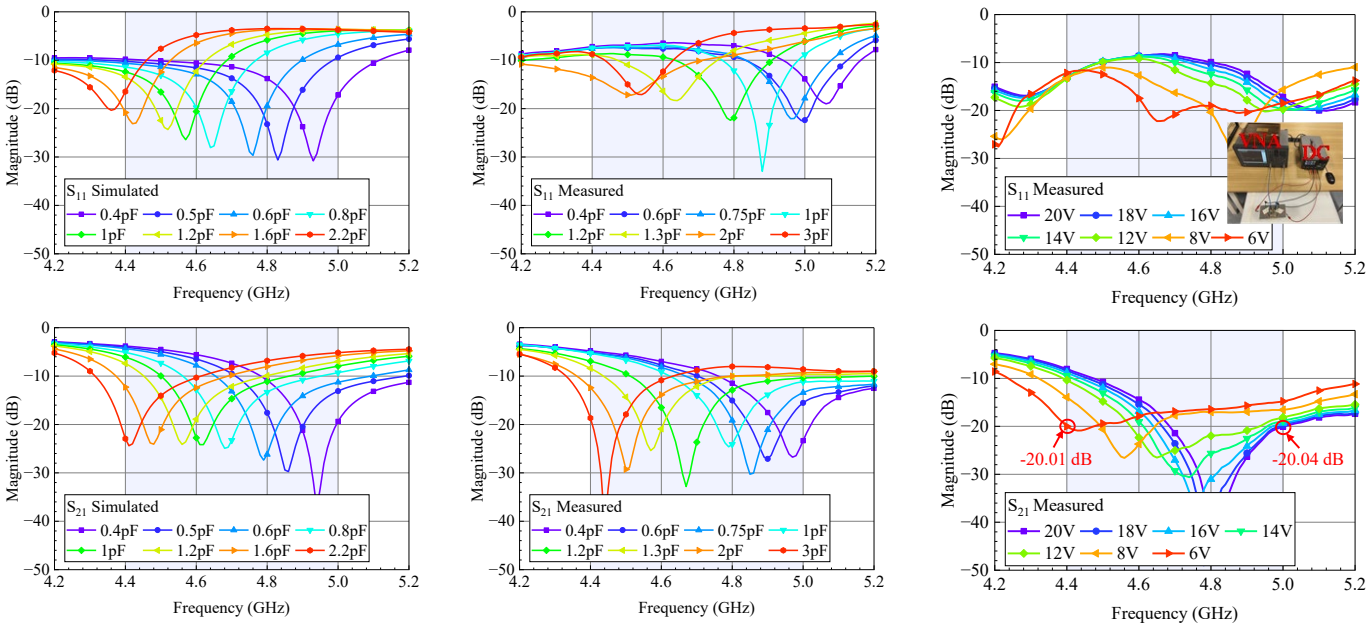

Fig. 7. Simulated and measured S-parameters of the proposed antenna. (a) Simulated. (b) Measured with discrete capacitors. (c) Measured with varactor diodes.

TABLE I
COMPARISONS OF SOME PRIOR AND THE PROPOSED METAL-BEZEL ANTENNA IN MOBILE TERMINALS

Ref.	Frequency Tunable	Self-Decoupled	Slit-Free	Radiator -Shared	Frequency Band (GHz)	In-Band Isolation	Measured Total Efficiency	Physical Size
[14][2023]	Yes	N. A.*	No	Yes	0.704 – 0.96 1.71 – 2.69 3.4 – 3.6	N. A.	> 33% > 46% > 43%	Folded copper plate: 113mm(total)×3mm
[16][2026]	Yes	N. A.	No	Yes	1.585 – 1.615 2.085 – 2.120 3.480 – 3.520	N. A.	44% – 83% 50% – 67% 51% – 63%	49.22×39.75×3.79mm³
[18][2017]	Yes	No	Yes	No	0.824 – 0.96 1.7 – 2.7	> 17 dB > 20 dB	> 43% 59% – 72%	145mm×72mm
[37][2020]	No	No	No	Yes	3.3 – 5	> 21 dB	58.9% – 88.6 % 31.6% – 76.7 %	40mm×3mm
[39][2019]	No	Yes	No	Yes	3.4 – 3.6	> 20.1 dB	35.2% – 64.7%	25×7×1.5mm³
[40][2024]	No	Yes	No	Yes	3.4 – 3.6	> 16.7 dB	54 – 65%	2×60.4×0.8mm³
This work	Yes	Yes	Yes	Yes	4.8 – 5 4.4 – 5 (Tunable)	> 20 dB > 20 dB	70.5% – 80.9% ~ 60 %	50mm×5.5mm 40mm×5.5mm

* N. A. denotes not applicable.

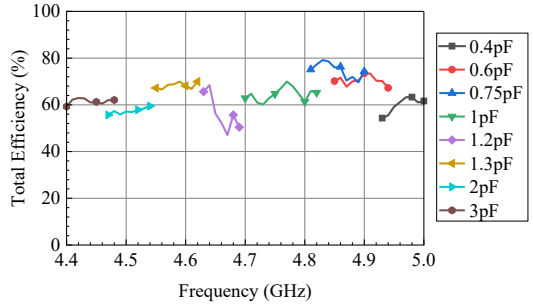

Fig. 8. Measured total efficiency of the proposed antenna using discrete lumped capacitors.

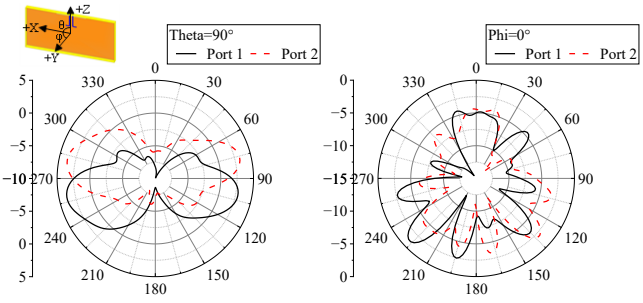

Fig. 9. Measured radiation patterns. (a) XOY plane. (b) XOZ plane.

proposed antenna allows the antenna to be placed in locations that are typically unavailable for traditional antennas with bezel slits, effectively trading a planar dimension for enhanced placement freedom and structural integrity.

IV. CONCLUSION

In this letter, by capacitively exciting an unbroken metal bezel at the proper position to adjust the mode impedances, an inherent self-decoupling is achieved, benefiting from the fact that the CM and DM share a similar dominant mode. Furthermore, by adjusting the equivalent length of the unbroken metal bezel through loading two varactor diodes, the working frequency of CM and DM so that the S_{11} and S_{21} can be simultaneously adjusted. A design example working in the N79 band from 4.4 to 5 GHz is presented, with isolation higher than 20 dB, matching condition better than -10 dB, demonstrating a promising candidate in mobile terminals for frequency-reconfigurable metal-bezel MIMO antennas.

REFERENCES

[1] Mobile Phone iPhone 4. Accessed: Jul. 18, 2025. [Online]. Available: https://support.apple.com/en-us/112562

[2] Y. Wang, L. Sun, Z. Du, and Z. Zhang, "Review antenna design for modern mobile phones: A review," *Electromagn. Sci.*, vol. 2, no. 2, pp. 1–36, Jun. 2024

[3] K.-L. Wong and C.-Y. Tsai, "Low-profile dual-wideband inverted-T open slot antenna for the LTE/WWAN tablet computer with a metallic frame," *IEEE Trans. Antennas Propag.*, vol. 63, no. 7, pp. 2879–2886, Jul. 2015.

[4] Y.-L. Ban, Y.-F. Qiang, Z. Chen, K. Kang, and J.-H. Guo, "A dual-loop antenna design for hepta-band WWAN/LTE metal-rimmed smartphone applications," *IEEE Trans. Antennas Propag.*, vol. 63, no. 1, pp. 48–58, Jan. 2015.

[5] H. Chen and A. Zhao, "LTE antenna design for mobile phone with metal frame," *IEEE Antennas Wireless Propag. Lett.*, vol. 15, pp. 1462–1465, 2016.

[6] Y. Liu, J. Zhang, A. Ren, H. Wang, and C. Sim, "TCM-based hepta band antenna with small clearance for metal-rimmed mobile phone applications," *IEEE Antennas Wireless Propag. Lett.*, vol. 18, no. 4, pp. 717–721, Apr. 2019.

[7] C. Deng, Z. Xu, A. Ren, and S. V. Hum, "TCM-based bezel antenna design with small ground clearance for mobile terminals," *IEEE Trans. Antennas Propag.*, vol. 67, no. 2, pp. 745–754, Feb. 2019.

[8] X. Tian and Z. Du, "Dual-feed shared-radiator metal-frame full-screen mobile phone antenna for GPS and LTE bands with a dual-function capacitor," *IEEE Trans. Antennas Propag.*, vol. 71, no. 10, pp. 8314–8319, Oct. 2023.

[9] P. Li, M. Hu, Y. Zhang, P. Liang, K. Wei, and Y. Li, "Wide-Beam metallic bezel antenna for direct satellite-to-handset communications," *IEEE Trans. Antennas Propag.*, vol. 73, no. 10, pp. 7370–7378, Oct. 2025.

[10] W. Zheng, Y. Yang, Y. Wang, C. Ding, and H. Li, "Turnkey automated design of handset antenna systems for enhanced cellular and SATCOM performance based on internal multiport method," *IEEE Trans. Antennas Propag.*, vol. 74, no. 1, pp. 337–350, Jan. 2026.

[11] M. Stanley, Y. Huang, H. Wang, H. Zhou, Z. Tian, and Q. Xu, "A novel reconfigurable metal rim integrated open slot antenna for octa-band smartphone applications," *IEEE Trans. Antennas Propag.*, vol. 65, no. 7, pp. 3352–3363, Jul. 2017.

[12] Q. Chen, J. Ala-Laurinaho, A. Khripkov, J. Ilvonen, R. M. Moreno, and V. Viikari, "Varactor-based frequency-reconfigurable dual-polarized mm-Wave antenna array for mobile devices," *IEEE Trans. Antennas Propag.*, vol. 71, no. 8, pp. 6628–6638, Aug. 2023.

[13] Q. Chen et al., "Single ring slot-based antennas for metal-rimmed 4G/5G smartphones," *IEEE Trans. Antennas Propag.*, vol. 67, no. 3, pp. 1476–1487, Mar. 2019.

[14] W. Zhao and Y. Wang, "A reconfigurable antenna with one slit and a small clearance for nona-band metal-bezel mobile phones," *IEEE Trans. Antennas Propag.*, vol. 71, no. 9, pp. 7172–7183, Sep. 2023.

[15] J. Choi, W. Hwang, C. You, B. Jung, and W. Hong, "Four-element reconfigurable coupled loop MIMO antenna featuring LTE full-band operation for metallic-rimmed smartphone," *IEEE Trans. Antennas Propag.*, vol. 67, no. 1, pp. 99–107, Jan. 2019.

[16] H. Zhu, N. Ma, D. Sun, Y. Gao, and S. Gao, "A tri-band frequency-reconfigurable endfire circularly polarized antenna in metal-rimmed phones for satellite communications," *IEEE Trans. Antennas Propag.*, vol. 74, no. 1, pp. 184-194, Jan. 2026.

[17] X. Chen, S. Zhang, and Q. Li, "A review of mutual coupling in MIMO systems," *IEEE Access*, vol. 6, pp. 24706–24719, 2018.

[18] Z.-Q. Xu, Y. Sun, Q.-Q. Zhou, Y.-L. Ban, Y.-X. Li, and S. S. Ang, "Reconfigurable MIMO antenna for integrated-metal-rimmed smartphone applications," *IEEE Access*, vol. 5, pp. 21223–21228, 2017.

[19] S. Zhang and G. F. Pedersen, "Mutual coupling reduction for UWB MIMO antennas with a wideband neutralization line," *IEEE Antennas Wireless Propag. Lett.*, vol. 15, pp. 166–169, 2016.

[20] M. Li, L. Jiang, and K. L. Yeung, "Novel and efficient parasitic decoupling network for closely coupled antennas," *IEEE Trans. Antennas Propag.*, vol. 67, no. 6, pp. 3574–3585, Jun. 2019.

[21] A. Zhang, K. Wei, Q. Guan, and Y. Hu, "Compactly placed high-isolated antenna pair with independent control of decoupling amplitude and phase," *IEEE Trans. Antennas Propag.*, vol. 71, no. 3, pp. 2814–2819, Mar. 2023.

[22] M. Li, Y. Zhang, D. Wu, K. L. Yeung, L. Jiang, and R. Murch, "Decoupling and matching network for dual-band MIMO antennas," *IEEE Trans. Antennas Propag.*, vol. 70, no. 3, pp. 1764–1775, Mar. 2022.

[23] G. Zhao et al., "A three-port coupled resonator decoupling network for mutual coupling reduction of three-element antenna arrays," *IEEE Trans. Microw. Theory Techn.*, vol. 72, no. 11, pp. 6585–6600, Nov. 2024.

[24] W.-F. Zeng, F.-C. Chen, and Q.-X. Chu, "Bandwidth-enhanced 5G mobile phone antenna pair with tunable electric field null," *IEEE Trans. Antennas Propag.*, vol. 71, no. 2, pp. 1960–1964, Feb. 2023.

[25] C. Deng, D. Liu, and X. Lv, "Tightly arranged four-element MIMO antennas for 5G mobile terminals," *IEEE Trans. Antennas Propag.*, vol. 67, no. 10, pp. 6353–6361, Oct. 2019.

[26] J. Sui and K.-L. Wu, "Self-curing decoupling technique for two inverted-F antennas with capacitive loads," *IEEE Trans. Antennas Propag.*, vol. 66, no. 3, pp. 1093–1101, Mar. 2018.

[27] J. Sui, C. Huang, and Y. F. Cheng, "Multi-element fully-decoupled inverted-F antennas for mobile terminals," *IEEE Trans. Antennas Propag.*, vol. 70, no. 11, pp. 10076–10085, Nov. 2022.

[28] K.-L. Wong, C.-Y. Tsai, and J.-Y. Lu, "Two asymmetrically mirrored gap-coupled loop antennas as a compact building block for eight-antenna MIMO array in the future smartphone," *IEEE Trans. Antennas Propag.*, vol. 65, no. 4, pp. 1765–1778, Apr. 2017.

[29] L. Liu, L. Zhao, Y. Cai, and Y. Yin, "Dual-feed MIMO antennas with one shared radiator for future 5G MIMO systems," in *Proc. 6th Asia–Pacific Conf. Antennas Propag. (APCAP)*, Xi'an, China, Oct. 2017.

[30] H. Chen, D. He, M. Zhang, and Y. Dou, "Self-decoupled coupled line antenna pair (CLAP)," *IEEE Antennas Wireless Propag. Lett.*, vol. 23, no. 10, pp. 2944–2948, Oct. 2024.

[31] J. Sui and K.-L. Wu, "A self-decoupled antenna array using inductive and capacitive couplings cancellation," *IEEE Trans. Antennas Propag.*, vol. 68, no. 7, pp. 5289–5296, Jul. 2020.

[32] X.-T. Yuan, Z. Chen, T. Gu, and T. Yuan, "A wideband PIFA-pair-based MIMO antenna for 5G smartphones," *IEEE Antennas Wireless Propag. Lett.*, vol. 20, no. 3, pp. 371–375, Mar. 2021.

[33] H. Li, Z. T. Miers, and B. K. Lau, "Design of orthogonal MIMO handset antennas based on characteristic mode manipulation at frequency bands below 1 GHz," *IEEE Trans. Antennas Propag.*, vol. 62, no. 5, pp. 2756–2766, May 2014.

[34] C. F. Ding, X. Y. Zhang, C.-D. Xue, and C.-Y.-D. Sim, "Novel pattern-diversity-based decoupling method and its application to multielement MIMO antenna," *IEEE Trans. Antennas Propag.*, vol. 66, no. 10, pp. 4976–4985, Oct. 2018.

[35] Y.-F. Cheng and K.-K. M. Cheng, "Decoupling of two-element printed-dipole antenna array by optimal meandering design," *IEEE Trans. Antennas Propag.*, vol. 68, no. 11, pp. 7328–7338, Nov. 2020.

[36] L. Sun, Y. Li, Z. Zhang, and H. Wang, "Self-decoupled MIMO antenna pair with shared radiator for 5G smartphones," *IEEE Trans. Antennas Propag.*, vol. 68, no. 5, pp. 3423–3432, May 2020.

[37] L. Sun, Y. Li, Z. Zhang, and Z. Feng, "Wideband 5G MIMO antenna with integrated orthogonal-mode dual-antenna pairs for metal-rimmed smartphones," *IEEE Trans. Antennas Propag.*, vol. 68, no. 4, pp. 2494–2503, Apr. 2020.

[38] H. Xu, S. Gao, H. Zhou, H. Wang, and Y. Cheng, "A highly integrated MIMO antenna unit: Differential/common mode design," *IEEE Trans. Antennas Propag.*, vol. 67, no. 11, pp. 6724–6734, Nov. 2019.

[39] L. Chang, Y. Yu, K. Wei, and H. Wang, "Polarization-orthogonal co-frequency dual antenna pair suitable for 5G MIMO smartphone with metallic bezels," *IEEE Trans. Antennas Propag.*, vol. 67, no. 8, pp. 5212–5220, Aug. 2019.

[40] Y. Fang, Y. Jia, J. Q. Zhu, Y. Liu, and J. An, "Self-decoupling, shared-aperture, eight-antenna MIMO array with MIMO-SAR reduction," *IEEE Trans. Antennas Propag.*, vol. 72, no. 2, pp. 1905–1910, Feb. 2024.

[41] X. Lu, H. Meng, and J. Sui, "Three examples of a frequency-reconfigurable radiator-shared metal-bezel MIMO antenna," IEEE Dataport, April 21, 2026, doi:10.21227/kex6-yf54.